HOLLOW CATHODE THRUST MEASUREMENTS USING A TARGET: INITIAL RESULTS AND SOME ISSUES

Paolo Gessini, Stephen B. Gabriel
Astronautics Research Group
School of Engineering Sciences
University of Southampton
Highfield, Southampton
Hants, SO17 1BJ
United Kingdom
pg4 | sbg2 @soton.ac.uk

David G. Fearn
EP Solutions
Fleet
Hants, GU14 0LX
United Kingdom
dg.fearn@virgin.net

ABSTRACT

A target system has been developed for the measurement of the thrust produced by a T6 hollow cathode and of its bulk plume current. Various issues connected with the experimental work have been explored with analytical and numerical tools. Initial results are presented and compared with theoretical predictions. Agreement is excellent for cold thrust (no discharge) measurements, especially at lower mass flow rates. With the discharge on, the thrust measurement is affected by thermo-mechanical problems. With the target operating as a Faraday plate, sizable currents have been collected. System reliability and accuracy limitations need to be addressed by a different design and the use of more accurate detectors.

INTRODUCTION

Hollow cathodes (HCs) are fundamental components of electron-bombardment ion thrusters. As such, their operation has been extensively investigated for decades. During some of these investigations, ions of sufficient energy to cause significant sputtering have been detected. In addition, it has also been observed that, in certain regimes, HCs can ionise a high fraction of propellant. Lately, efforts have been made by different investigators to obtain more detailed measurements, understand the mechanisms behind the generation of these high-energy ions and assess the possibility of using them to produce thrust[1,2,3,4,5]. Modelling HC operation is also an ongoing activity at several institutions[1,2,3,5,6,7,8].

By gaining a deeper insight into the ion-emission characteristics of a HC, a simple non-magnetic micro-ion thruster could be built using well-tested technology. To this end, an indirect thrust measurement system, consisting of a Cantilever Beam Target (CBT), impacted by the HC plume, and a Laser Optical Lever (LOL) measuring its angular deflection, has been developed at the University of Southampton.

In a previous paper[1], through a critical review of experimental results available in the literature, the authors estimated the ion flux and hence the thrust that can be obtained. They also reported some measurements of the momentum flux produced by a HC designed for the T6 ion thruster[13], performed at QinetiQ (formerly DERA) with a target balance.

In a more recent paper[2] the development of the system consisting of the CBT and the LOL was described. A direct calibration was performed with accurately measured weights, confirming that the system conforms to the theory of slender beams to a great degree of accuracy for loads equivalent to thrusts into the sub-mN range.

In this paper, a more detailed understanding of the CBT behaviour, obtained with both analytical and numerical tools, is presented. Initial measurements of ion momentum and mass flow rate (thrust and collected current) are reported. Cold-gas thrust measurements, obtained with no discharge, are compared with analytical predictions from choked orifice gas dynamics and free-molecular flow and with numerical simulations, performed with a code[14,15] currently under development at the University of Southampton.

THE CBT-LOL MEASUREMENT SYSTEM

The CBT

In the two previous papers[1,2] published on this subject, we reported a description of our CBT, consisting of a thin beam connected to a square target, manufactured from a single piece of Al 3003 sheet, and a very simple static analysis, following the theory of slender beams. The analytical calculations were double-checked by running simulations in ANSYS®, a finite element analysis program. We obtained an expression for the sensitivity (angular deflection per unit force), which was confirmed, to a high degree of accuracy, by a direct calibration[2]. This was performed with accurate weights and our LOL in a horizontal position. By measuring deflections from the equilibrium position of the beam under its own weight and the new positions obtained after adding calibrated weights on it, it was concluded that we could neglect the effect of gravity, due to the linearity of elastic deformations.

Once the CBT is mounted vertically inside the vacuum chamber, during the actual HC thrust measurement, the effect of gravity becomes important. The equilibrium configuration to which the device will tend, after a transient, is determined by the HC thrust and by the target weight, producing bending moments of opposite sign. Therefore, gravity will effectively decrease the deflection caused by a certain force and thus the target sensitivity as any deflection will give rise to a bending moment countering the deflection itself.

The differential equation describing the behaviour of a cantilever beam subjected to a concentrated load F, perpendicular to the beam axis at $z = L + D/2$ is[9]

$$\frac{d^2 y}{dz^2} = \frac{F}{EI}\left(L + \frac{D}{2} - z\right), \tag{1}$$

where z is the distance along the beam axis and $y(z)$ the displacement perpendicular to it. D is the target diameter, or its side in the case of a square target, like the one used in these initial experiments. E is the Young's modulus of the material used and I the moment of inertia of a beam cross-section about the neutral axis[9]. This equation can be immediately integrated with the boundary condition $dy/dz = 0$ for $z = 0$. The angular deflection at $z = L$ is

$$\frac{dy}{dz} = 6\frac{F}{Ebh^3} L(L + D), \tag{2}$$

where b and h are, respectively, the width and thickness of a beam with rectangular cross-section and we have substituted $I = bh^3/12$. By setting $dy/dz = \Delta\theta$ for $z = L$, we can write the sensitivity as:

$$\frac{\Delta\theta}{F} = \frac{6}{Ebh^3} L(L + D). \tag{3}$$

This is the equation used throughout our direct calibration[2]. It describes the behaviour of our CBT quite appropriately, as the target itself, for $z > L$, having a much greater width, can be considered rigid compared to the beam ($z \quad L$). The angular deflection $\Delta\theta$ is then constant for $z \quad L$ and the actual distribution of the applied load is irrelevant, as long as we can assume it is symmetric with respect to the target. We can then use the equivalent concentrated load F applied at the target centre. The load on the beam, with a small frontal area and far away from the HC axis, will be negligible, as very few particles will impinge on it.

If we now consider the cantilever beam mounted vertically and include the effect of the weight as a distributed load, the differential equation describing its behaviour changes substantially. Assuming instead the weight of the beam to be negligible compared to the weight of the target itself, which is reasonable for our geometries, we can model it simply as a load $W = \rho ghD^2$ concentrated at the centre of the rigid target. Here, ρ is the density of the material and g the acceleration of gravity at sea level. As the beam deflects, the target experiences a rotation $\Delta\theta$ and its centre a displacement $y(L+D/2) = \Delta y$. For small values of the angle

Äè, the load *F* will still be perpendicular to the target *(F cos Äè ~ F).* Thus it can be shown that Equation 1 is modified by the addition of a bending moment term, yielding

$$\frac{d^2y}{dz^2} = \frac{1}{EI}\left[F\left(L + \frac{D}{2} - z\right) - W(\Delta y - y)\right], \tag{4}$$

which can be rewritten as

$$\frac{d^2y}{dz^2} - \frac{W}{EI}y = \frac{1}{EI}\left[F\left(L + \frac{D}{2} - z\right) - W\Delta y\right]. \tag{5}$$

This equation can still be solved analytically by treating *Äy* as an unknown parameter, yielding *y(z)* as a function of *Äy*. Then, remembering that, under the assumption that the target is rigid compared to the beam, we have *dy/dz = Äè = const* for *z L*, we can write the displacement of the target centre as

$$\Delta y = y(L) + \Delta\boldsymbol{q}\frac{D}{2}\ . \tag{6}$$

By substituting into this equation the expressions for *y(L)* and *dy/dz(L) = Äè*, obtained from the solution of Equation 5, and then solving for *Äy*, we obtain an expression that we can then substitute back into the expression for *dy/dz(L) = Äè*, obtaining, for the sensitivity of our CBT:

$$\frac{\Delta\boldsymbol{q}}{F} = \frac{1}{W}\Psi(L, D, E, h, b, g, \boldsymbol{r}), \tag{7}$$

where *Ø* is a function of the CBT geometry and material properties. From this expression it can be immediately seen that, for *F >> W*, the effect of the weight can be neglected. As *W* increases, gravity will contrast the moment produced by *F*, decreasing the bending of the beam. For our CBT geometry and material (Al 3003), Equation 3, appropriate during the calibration, yields for the sensitivity a value *Äè/F = 1.60 ìrad/ìN*. Equation 7, appropriate during the actual thrust measurements, yields *Äè/F = 1.23 ìrad/ìN*. If we used the uncorrected value from the simple Equation 3, we would be underestimating our thrust by 23%. The introduction of this correction is only necessary when the CBT is mounted in a vertical position, as it was during the experiments reported in the present paper. In order to decouple the effect of the target weight and of the HC thrust, in future experiments a different configuration will be tested, with the CBT rotated by 90 with respect to the present set-up. In this way, the moments produced by F and W will act perpendicularly to each other. With a beam which is much wider than thicker, the bending caused by the weight will become negligible, as the moment of inertia around the neutral axis is $I = bh^3/12$ and what is the width for F is thickness for W. For the CBT used in these experiments, the sensitivity to bending by the weight, calculated using the simple beam equation 3, would be 25 times as small. This could be easily increased with slight changes in the beam geometry but, as the two deflections are now decoupled, the thing would hardly be necessary, as the weight would no loner cause an error in the thrust measurement.

The CBT-LOL measurement system was originally designed with the purpose of measuring the static response of a beam to an applied load. In order to address the issues detailed in the chapter on hot thrust and alleviate the problems related to thermal stresses, it was decided not to operate the HC for extended periods of time. By operating the HC in short "bursts", the oscillations of the CBT do not have time to converge to the static solution due to damping: a transient analysis becomes then more appropriate. In the initial results presented in this paper, the displacement is the average of the extremes of the laser spot oscillations, measured visually on a screen.

The time necessary for the oscillations to be effectively damped depends essentially on the beam geometry and material properties, namely density, Young's modulus and a damping coefficient. Several models have been developed to address this phenomenon. In the theory of hysteretic damping, a loss factor ç is introduced according to which the oscillations decrease exponentially. Aluminium, with ç = 0.0001 – 0.0006, is one of the metals with the lowest damping. This produced very persistent oscillations during our first experiments. Recently, dynamic transient simulations have been run in ANSYS®. These show that the transient oscillations actually converge to a steady-state solution that can be determined with a static analysis. Unfortunately, due to the difficulties involved in accurately modelling the damping, it has not been possible to progress beyond qualitative indications. However, it has been noted experimentally that the oscillations have a frequency of the order of the Hz, which can be followed easily by the naked eye. After a few seconds, their amplitude has decreased enough to confidently determine the static response as described above.

The LOL

An exhaustive description of the LOL principle of operation was presented in a previous paper[2]. This straightforward and robust instrument translates the CBT angular deflection *Äè* into a linear displacement *Äx*, according to the formula

$$\Delta x = 2L\Delta\theta, \tag{8}$$

which shows that the sensitivity of this instrument can be increased at will by increasing the optical path length *L*, the only limitation being the divergence of the laser beam.

THE EXPERIMENTAL APPARATUS

The Vacuum Rig

The vacuum rig used in all our experiments is, essentially, that constructed by Edwards[10] and modified by Milligan[11]. High vacuum ISO and CF flanges are employed throughout the chamber. Pumping is achieved by the use of a rotary and a turbo-molecular pump connected in series. In order to avoid oxygen poisoning of the HC, a background pressure in the 10^{-7} mbar range has to be reached prior to commencing an experimental run. Depending on the set-up, this may require running the pumping system overnight.

The T6 Hollow Cathode / Anode Assembly

The HC investigated at the University of Southampton is the one designed for the T6 Kaufman-type ion thruster[13]. The basic features of this cathode have essentially remained unchanged since the start of the development programme and are described, together with the physics of HC operation, in numerous papers[1,3,12,13]. The initial orifice diameter of this HC was 0.5 mm. This is a smaller value than those used in most measurements by other investigators, as the orifice diameter is one of the parameters the influence of which on the ion emission and the thrust we intend to explore. However, after the experimental runs described in this paper, a certain amount of erosion is already visible. It has been observed in various experiments that, when operating a T6 HC at discharge currents above 10 A, a small orifice will quickly erode until it attains a diameter of about 0.7-0.8 mm.

In these initial experiments the HC was operated in an open-diode configuration, without using a keeper electrode. A circular anode, manufactured from a 100-mm diameter stainless steel disc, with a 10-mm diameter central orifice, was mounted at ~ 4.5 mm in front of the HC tip. Intense heating of the anode was observed, especially when operating in a plume mode. A visual examination of the anode face after many experimental runs revealed the presence of tantalum, sputtered from the HC tip. This was confirmed by an accurate Scanning Electron Microscope (SEM) analysis.

The Target Assembly

The CBT is mounted on an L-shaped support, connected to a UK-25 ion thruster backplate. It is positioned in front of the HC / anode assembly, with the centre of the square target on the axis of radial symmetry. Through a micro-translation mechanism it is possible to finely adjust the target distance from the HC. The mechanism itself can be mounted at different positions on the support. This is important, as measurements of the angular distribution of ion current show that, while most of the ions escape from the HC / keeper assembly at angles <30º, significant amounts are still present at higher angles[1,2,5]. Therefore, positioning the target too far away from the HC would entail underestimating the thrust. In the experiment reported in the present paper, the target was mounted at ~ 55 mm from the anode.

Two distinct targets were used during the experiments described in this paper. From now on, they will be referred to as First-Generation Target (1GT) and Second-Generation Target (2GT). The 1GT was described in previous papers[1,2]. The 2GT has identical geometry, a square target with D = 100 mm connected to a thin beam with b = 4 mm and L = 150 mm, manufactured as a single piece from Al 3003 sheet of Al 3003 with h = 0.8 mm. The only difference is that the free end of the beam, beyond the target, has been eliminated. It had been included in the original design in order to increase the displacement of the end of the beam, thus increasing the measurement resolution. As it was later decided to measure the angular deflection instead, and this is constant beyond the position where the load is applied, the end part of the beam became unnecessary. A more important difference is that in the 1GT the reflection of the laser beam from the backside of the target was obtained by attaching a thin mirror to it with a special, temperature-resistant cement. This method proved to be unreliable, though, as in one instance the mirror actually detached and fell off the target. Even if this was probably due to an imperfect curing of the cement, the investigators feared that small movements of

the mirror with respect to the target, while not so dramatic, would introduce an additional source of error into the measurement. It was therefore decided to polish the backside of the target to a mirror quality. This gave satisfactory results, as the reflection from this Al mirror did not seem to appreciably affect the beam divergence and intensity.

The Optical Set-Up

A version of our LOL has been set up with components both inside and outside the vacuum chamber. It consists of a green He-Ne laser mounted externally, two convex lenses forming a Keplerian beam expander and four mirrors, one of which is the polished backside of the target, not facing the HC. These mirrors direct the laser beam onto the target inside the chamber and then the reflected beam outside, along an optical path with a length L = 9.0 m (1GT experiments) and L = 9.2 m (2GT experiments). The total displacement of the laser beam is read visually on a screen through a scale with a 0.5-mm resolution.

The Electrical Set-Up

During the experimental runs described in the present paper, the HC was kept at ground potential. The anode was connected to a current-regulated power supply, with the potential limited at 80 V maximum. The target was connected to several power supplies, connected in series or in parallel, in order to allow current collection at different bias potentials, both positive and negative. The collected current is passed through a multimeter and measured with a resolution of 1 mA.

INITIAL RESULTS AND DISCUSSION

Plume Current

The target has also been used as a Faraday plate, to collect the total current in the plume. By biasing it at different potentials, electron and ion currents can be measured. Figure 1 shows a typical V-I characteristic of

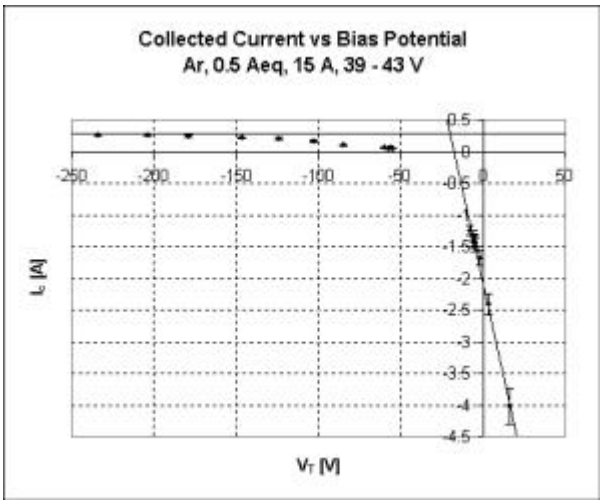

Figure 1 – Target V-I characteristic.

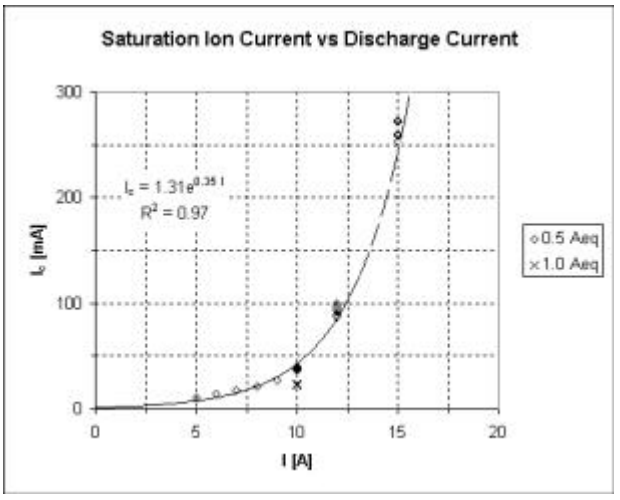

Figure 2 – Saturation collected ion current.

the target acting, in effect, as a Langmuir probe, during a single experimental run. For increasingly negative potentials, saturation of the collected ion current branch is evident. As the bias potential becomes positive, large electron currents are drawn by the probe. The target now becomes effectively a second anode, being of comparable size. This changes the discharge conditions, causing the anode voltage to vary. In addition to this, heating led to one of the 1GTs being seriously damaged. This accounts for the region of missing data in the curve in the electron-current saturation region. A positively biased target, therefore, alters the discharge considerably, while a negatively biased target, drawing a much smaller current, leaves it substantially unchanged. This is shown by the variation of anode voltage, which, for a target bias potential between - 50 and - 230 V, is only about ± 5 % for a single run. Such behaviour suggests that we can use a large biased target, relatively close to the anode, to collect bulk current measurements with just small alterations of the discharge parameters.

The saturation ion current increases exponentially with increasing discharge current (see Figure 2). For the same discharge current, increasing the mass flow rate will result in a smaller value of collected ion current and therefore, assuming that Ar is singly ionized, ion flow rate, suggesting a lower ionization fraction. This

could be explained by the fact that, at 10 A discharge current, anode voltages are ~ 40 V at 0.5 Aeq flow rate and only ~ 20 V at 1.0 Aeq. This means that the average power per particle available in the discharge decreases by a factor of four. It has not been possible to establish a clear correlation between an increase in the current collected, as we approach saturation by increasing the bias voltage, and an increase in the thrust measured. This may suggest that, as we increase the target bias potential and its sheath expands, more low-energy ions are extracted from the plasma and collected. This would increase the current measured, while the thrust, due mainly to hot neutrals and a small amount of high-energy ions, would be substantially unaffected.

Cold Thrust (Discharge Off)

Numerous measurements were performed of the thrust generated by the flow through the HC with no discharge, both with the 1GT and the 2GT. No appreciable difference was noticed between the two targets. Each data point shown in Figure 3 is an average of several measurements. The error bars represent systematic errors due to uncertainties in the various measurements involved in the calculation, dominated by the error in the visual reading of the laser spot displacement on a scale with a ± 0.5 mm resolution.

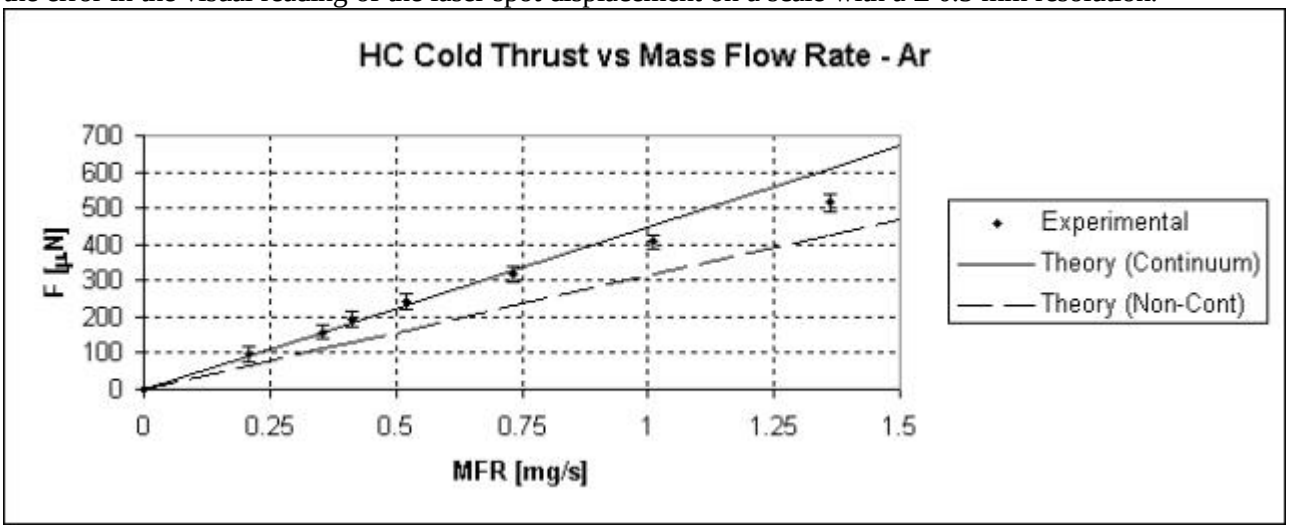

Figure 3 – HC cold thrust (no discharge, no heating) vs mass flow rate.

The measured thrust shows good agreement with theoretical predictions, with a dependence on mass flow rate (MFR) essentially linear, especially for MFR 0.5 mg/s. The slight drop in thrust at higher values of MFR might be due to plume geometry effects and its interaction with the target. In the orifice we have $Kn \sim 10^{-2}$, where $Kn = \ddot{e} / d$ is the Knudsen number. $\ddot{e}$ is the mean free path and d the orifice diameter. This means that we should be in a regime of continuum flow, or better slip flow, at least inside the HC. Continuum-flow theory predicts, for a choked, sonic orifice, a specific impulse[22]

$$\frac{F}{\dot{m}g} = I_{sp_c} = \frac{1}{g}\left(2\frac{\tilde{a}+1}{\tilde{a}}\frac{kT}{m}\right)^{\frac{1}{2}}, \qquad (9)$$

where $\dot{m}$ is the MFR, $\tilde{a}$ the ratio of specific heats, k the Boltzmann constant, T the temperature and m the atomic mass. This is plotted as the solid line in the graph: the agreement with experimental data is excellent. Free-molecular, non-continuum flow theory yields a lower value[23]

$$\frac{F}{\dot{m}g} = I_{sp_{nc}} = \frac{1}{g}\left(\frac{\pi}{2}\frac{kT}{m}\right)^{\frac{1}{2}}, \qquad (10)$$

which is only ~ 70% of that predicted by continuum theory. Equation 10 underestimates the thrust, but is drawn in the graph as a dashed line for comparison. In order to corroborate the continuum flow analysis that predicts choking at the orifice for a large range of flow conditions, numerical simulations were performed using a DSMC code developed at the University of Southampton[15] in order to simulate the experimental configuration used in these experiments. They confirm, at MFR = 0.414 mg/s = 1 Aeq of Ar, T = 300 K, the presence of a sonic line at the orifice. Slip at the wall has been actually "seen" in some simulations[15].

Hot Thrust (Discharge On)

When the HC discharge is initiated, a large increase in the LOL beam displacement is measured. However, the initial results are complicated due to heating, causing thermal expansion of the target and change in the

material properties with temperature. These problems had been in part anticipated[1,2] and are at present being analyzed and modelled.

The flux of energy into the target is due to radiation from the hot HC tip and the anode and to the impacts from the plume particles, both charged and neutral. If the target has a strongly negative bias, the energetic ion contribution can become important. In order to reduce the heat flux, it was decided to operate the HC in a "pulsed" mode. Instead of having a steady discharge on for hours at a time, changing parameters like current and mass flow rate, the device was turned on for short periods of time, of the order of a minute or less. This raises the issue of whether this operation is substantially identical to the ordinary steady one. The temperature of the various components (HC, anode, target), in particular, will be strongly history-dependent, if the system is not allowed to reach thermal equilibrium. This affects the discharge characteristics, like for example the anode voltage, which tends to fluctuate.

Figure 4 shows the first hour of a typical experimental run. After an initial displacement due to the cold thrust, we see the spot moving slowly upwards from time $t = 0$, when we turn on the HC heater, to the time when the discharge is switched on for the first time and the heater off, after reaching a steady-state temperature condition. Then there is a quick upward movement, the discharge is given several seconds to get established and then is switched off. A quick descent of the laser spot is then followed by a slower movement, until the next "burst". The displacement that we measure here is due in part to the momentum transferred from the plume particles to the target, but is also affected by two sources of error. Namely, the variation of the material properties, in particular the Young's modulus, and the thermal expansion due to the temperature rise produced in the target by the HC operation.

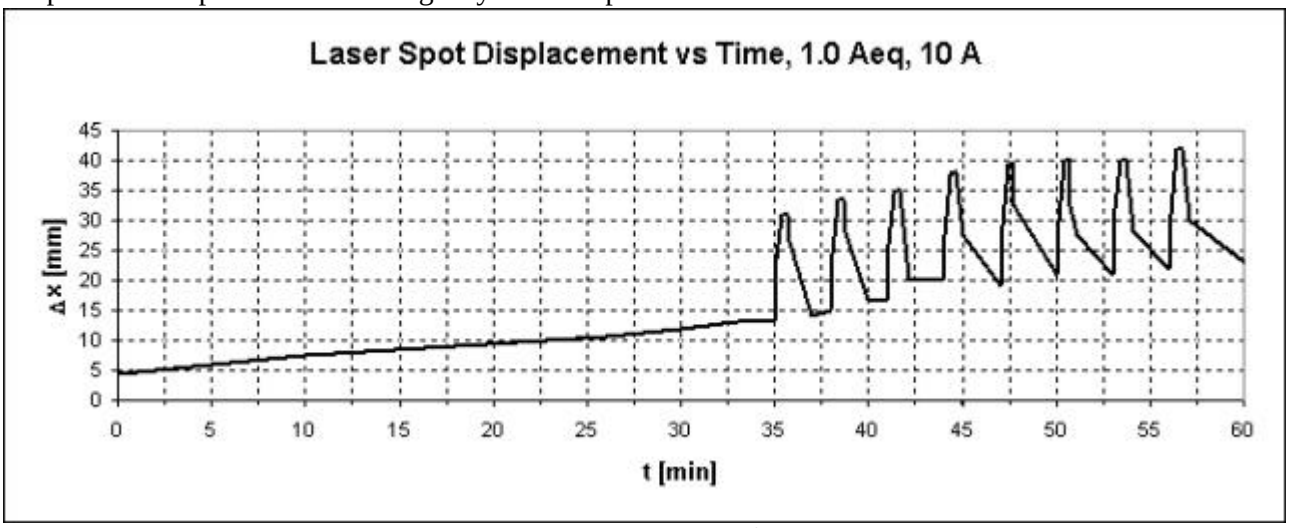

Figure 4 – Displacement time history of an experimental run.

From a physical point of view, our target will tend to deform because the face receiving the heat flux from the HC will be at a higher temperature than the other one, radiating into a vacuum at room temperature. The thermal expansion will be therefore lower on the colder face. This will cause the CBT to bend and bring about an overestimation of the thrust deflection.

From Equations 3 and 8, we see that the sensitivity of our CBT is inversely proportional to E and that the laser spot displacement Δx is proportional to the angular deflection $\Delta\theta$. We can thus write, for the displacement we actually measure on the screen, Δx_m:

$$\Delta x_m = \frac{E_c}{E_h}\,\Delta x + \Delta x_{te}\ , \tag{11}$$

where E_c is the Young's modulus at room temperature and E_h its value after the temperature increase. Δx_{te} is the additional displacement that we will measure due to thermal deformation (differential expansion) of the target. In order to estimate the various terms in this equation, we need to assess the temperature increase of the target and relate it to the variation in E and the thermal deformation. The Young's modulus E, in general, decreases with increasing temperature. This produces an increase in the sensitivity of our CBT (see Equation 3) and could lead to overestimating the thrust. For aluminium, this effect is quite linear between room temperature and ~ 300 C, with E decreasing from ~ 70 GPa to ~ 60 GPa.

In order to relate this angular deflection to the energy flux into the target, a model of the heat transfer and induced strains and stresses is necessary. This is an essentially three-dimensional problem and, as such, its solution is beyond the scope of the present paper. An order-of-magnitude estimate can be obtained with a simple one-dimensional heat transfer model and with an analytical calculation, involving elements of the elementary theory of beams and of strains and stresses induced by thermal gradients.

To go beyond a qualitative assessment, let us model our CBT as a cantilever beam subjected to a temperature gradient across its thickness *h*. The angular deflection *Äè* can be related to a position *l* along the beam and the difference in temperature *ÄT* between the two faces by the relation[9,16,17,18]

$$\Delta\theta = \frac{l}{h}\,\alpha\Delta T\,, \tag{12}$$

where *á* is the coefficient of linear reversible thermal expansion. *ÄT* can be estimated by modelling our CBT as a metal strip delimited by two parallel planes. In this case, analytical solutions can be obtained for various boundary conditions[19]. With a heat flux *Q* [Wm^{-2}] into one plane and radiation from the other plane into a background at the initial temperature, we have a transient heating to reach a steady-state temperature distribution which allows a drop *ÄT* across the thickness of the strip, due to the finite thermal conductivity K. Due to the high value of *K* for metals in general and aluminium in particular, *ÄT* is extremely small and is established very quickly, while the average temperature is still rising. Numerical calculations, performed with FEHT, a Finite Element Heat Transfer program, have allowed us to follow the transients to the steady states (reached after times *t* ~ 15'-30') and to confirm that including radiation from the hotter face in our model would sensibly reduce *ÄT*. This is a non-linear phenomenon, very sensitive to variations in temperature, radiation being proportional to T^4. By neglecting it as a first approximation, we can write as an upper estimate of the temperature drop across the metal strip[19]:

$$\Delta T = Q\frac{h}{K}\ . \tag{13}$$

Combining Equations 12 and 13 finally yields, for the CBT angular deflection:

$$\Delta\theta = Q\,l\frac{\alpha}{K}\ . \tag{14}$$

Equation 14 shows that, as a first approximation, the angular deflection does not depend on the beam thickness, as a thicker beam is more rigid but also allows a larger temperature drop across. As our CBT sensitivity is proportional to $1/h^3$ (see Equation 3), using a thin beam is advantageous anyway.

The heat flux into the target can be assessed as the sum of different contributions:

$$Q = \varepsilon_1\varepsilon_2 G\sigma T^4 + \frac{5}{2}kT\frac{\dot{m}}{m}\frac{1}{D^2} + \frac{I_i}{D^2}V_b\ . \tag{15}$$

Here *å* is the emissivity, *G* a geometric coefficient, *ó* the Stefan-Boltzmann constant, *k* the Boltzmann constant, $\dot{m}$ the MFR, I_i the ion current and V_b the target bias potential. The first term on the RHS of Equation 15 is the radiation heat flux, the second one the energy transported by the heavy particles, assumed in equilibrium with the HC tip, the third one the energy transported by the ions accelerated by the target bias voltage. Once we have estimated *Q* with Equation 15, we can calculate *T* analytically or numerically, the way we did using FEHT, and *ÄT* using Equation 13. Using data in the literature we can estimate the variation in *E*, as we did above. Using Equations 12 and 8, we can calculate $Äx_{te}$. In this way, from Equation 11 we obtain the effective *Äx* and the correct value for the thrust, through Equation 3 or 7.

From the displacement time history prior to the first HC discharge we can get an idea of the thermal effects, due to the slowly heating HC tip radiating onto the target through the anode orifice, some heating of the anode itself and heat convection from the plume argon atoms. In this case such effects can be estimated as the difference between the total displacement measured and the thrust exerted by the hot gas. From Equation 9, this will be equal to the cold thrust, measured without thermally-induced errors, times the square root of the ratio between hot HC tip temperature and room temperature. Data on typical T6 HC operation allow us to estimate the tip temperature at ~ 1500 K. With the cold thrust giving a *Äx* = 4.5 mm, we have a difference between the gasdynamic thrust *Äx* ~ 10 mm and the *Äx* actually measured (~13 mm) of ~ 3 mm.

Assuming a HC tip at 1500 K, heavy particles at the same temperature and an anode at 600 K, we obtain a heat flux Q ~ 200 - 400 Wm^{-2}, depending on the values we assume for the various emissivities. At room

temperature, E = 69 GPa for Al 3003. For Q = 400 Wm^{-2}, FEHT simulations show that, after 35 minutes, the beam will reach a steady-state temperature of 464 K, starting at T = 300 K. This means that now E ~ 62 GPa and the sensitivity of our CBT has gone up by ~ 11% (see Equation 3). This effect is dominant compared to the thermal bending. From Equations 8 and 14, using values of the thermal expansion coefficient $\acute{a}$ ~ 25×10^{-6} K^{-1} and thermal conductivity K ~ 160 $Wm^{-1}K^{-1}$ appropriate for our CBT material (Al 3003), this latter would account for a $Ä x_{te}$ of only ~ 0.24 mm.

Using Equation 11 we obtain, from the measured value $Ä x_m$ ~ 13 mm, a corrected value $Ä x$ ~ 11.5 mm. By comparing this with the calculated value of the hot gas thrust (~ 10 mm) we see that our correction is too small, by a factor of two. Considering the uncertainties in the actual value of the HC tip temperature and of the anode, very close to the HC tip and of area comparable to the target, as well as those in the values of the emissivities, we might well be underestimating the actual heat flux into the target. In particular, the emitter composed of the HC tip orifice viewed through the anode orifice, resembling a cavity, could have a much higher emissivity than that of tantalum, approaching a black body. A visual inspection of the anode after several experimental runs revealed the presence of sputtered material from the target (Al) and the HC tip (Ta). This was later confirmed by an accurate SEM exam of the anode surface. The target also shows clear traces of sputtering due to heavy-particle impacts. We know that rough surfaces can have emissivities, for the same material, even an order of magnitude higher than shiny ones. The above facts suggest that we might be greatly underestimating the power radiated into the target. The approximations involved in our simple heat transfer analysis of the target and of the thermal strains and stresses it endures, on the other hand, could lead us to overestimating the heat flux needed to cause a certain deflection of our CBT.

When the discharge is initiated, the HC tip and the propellant gas get hotter and the anode temperature is greatly increased by Joule heating and, predominantly, by the energy deposited by the electrons falling through the anode sheath potential. A plasma is created in the HC insert region and orifice, escaping through the anode orifice and impinging on the target. Now the power radiated into this latter goes up, as well as the energy transported into it by colliding heavy particles, both neutral and charged. The ions are accelerated by the target bias potential, thus increasing their energy. The gasdynamics thrust increases with the square root of temperature. Momentum is transferred to the target by the impacting ions. In addition to these phenomena, a $j\times B$ force accelerates the plasma, much in the same way as what happens in a magnetoplasmadynamic (MPD) thruster[20]. HCs have actually been used in MPD thrusters with good results[21]. The values of thrust produced were in agreement with those predicted by the classic formulation[20,21].

Once the discharge "bursts" start, the target is pulse-heated and its deformation increases. The LOL spot starts drifting upwards on the screen. Now the heat flux Q is larger, but we do not allow the system to approach thermal equilibrium. FEHT simulations with Q = 1500 Wm^{-2} give a steady-state T = 630 K after a time t ~ 22', starting at T = 300 K. During a pulse, there will only be a slight increase over the temperature reached with the heater. The $ÄT$ across the thickness, however, is established quickly, so that now we will have, from Equations 8 and 14, $Ä x_{te}$ ~ 1 mm. The first "burst" produces a $Ä x_m$ ~ 32 mm, with an increase over the $Ä x$ produced by the hot gas (with no discharge) of ~ 19 mm. Temperatures are uncertain, but assuming an increase in the target sensitivity of ~ 15% we have an estimate for the $Ä x$ actually produced by the thrust of ~ 27 mm. From Equations 7 and 8, we calculate a value of F ~ 1.2 mN. At a mass flow rate of 1 Aeq ~ 0.4 mg/s of Ar, this corresponds to a value of specific impulse I_{sp} ~ 300 s for our T6 HC at 10 A discharge current. This is a very approximate analysis, though: for the hot thrust with no discharge we were underestimating thermal effects by a factor of two.

CONCLUSIONS AND FUTURE WORK

A thrust and current measurement system, consisting of a cantilever beam target and a laser optical lever, has been developed, calibrated and tested with actual thrust and plume current measurements of a T6 hollow cathode. While the cold thrust measurements show excellent agreement with the theory, measurements of the hot thrust, with discharge on, have been complicated by thermal effects. In the future, though, changes in the target design, guided by accurate analytical and numerical modelling, will alleviate the thermal problems. A Position Sensitive Detector (PSD) has been purchased and will be implemented. This will increase the resolution of the displacement reading by two orders of magnitude. This increased resolution will render the use of long optical paths to magnify the laser spot movement unnecessary. This in turn will eliminate the need for a beam expander to decrease the beam divergence and limit the size of the laser spot. Another great

benefit will be the possibility to follow and record the time history of the laser beam movement with a visually unattainable accuracy, as the PSD time response is of the order of microseconds. This will give us the possibility to perform a transient analysis and compare it to the theory. A picoammeter will allow to greatly improve the resolution of our measurements. This will become necessary when using the ion probe described in a previous paper[2], which collect currents orders of magnitude lower, due to its small entrance aperture. This kind of probe will allow an accurate estimate of the ion energies and a spatially-resolved measurement of the plume current, to complement the bulk measurements obtained with the CBT.

REFERENCES

[1] Gessini, P, Gabriel, S B, Fearn, D G, IEPC-01-233 and References therein

[2] Gessini, P, Gabriel, S B, Fearn, D G, JPC-2002-4104 and References therein

[3] Patterson, S W, Fearn, D G, IEPC-99-125 and References therein

[4] Foster, J E, Patterson, M J, AIAA-2002-4102

[5] Crofton, M W, Boyd, I D, AIAA-2002-4103

[6] Rossetti, P, Paganucci, F, Andrenucci, M, AIAA-2002-4239

[7] Domonkos, M T, AIAA-2002-4240

[8] Katz, I, Anderson, J R, Polk, J E, Brophy, J R, AIAA-2002-4241

[9] Morley, A, "Strength of Materials", London: Longmans, Green and Co. Ltd., 1946.

[10] Edwards, C H, PhD Thesis, University of Southampton, August 1997.

[11] Milligan, D J, PhD Thesis, University of Southampton, March 2001.

[12] Patterson, S W, Jugroot, M, Fearn, D G, AIAA-2000-3532

[13] Wallace, N C, Mundy, D H, Fearn, D G, IAF Paper IAF-99-S.4.08, October 1999.

[14] Crawford, F T A, Gabriel, S B, AIAA-2002-2101

[15] Crawford, F T A, Gabriel, S B, IEPC-03-0027

[16] McGuire, W, Gallagher, R H, Ziemian, R D, "Matrix Structural Analysis", John Wiley & Sons, 2000

[17] Carl B. White, Private Communication

[18] Christoph Schwingshackl, Private Communication

[19] Carslaw, H S, Jaeger, J C, "Conduction of Heat in Solids", Oxford University Press, 1959

[20] Jahn, R G, "Physics of Electric Propulsion", McGraw-Hill, 1968

[21] Toki, K, "Quasisteady MPD Arcjet with Hollow Cathode", J. Propulsion, Vol. 2, No. 5, 1986

[22] Hill, P G, Peterson, C R, "Mechanics and Thermodynamics of Propulsion", Addison-Wesley, 1965

[23] Turchi, P G, "Molecular Theory of Gas Flow", Lecture Notes, The Ohio State University, 1996-1997